CHAPTER 4
A 1D MODEL OF SOLIDIFICATION ON THE SLAG BATH SURFACE

This chapter describes a dynamic one-dimensional model of the crust that forms on the slag bath surface when furnace inputs are switched off for extended periods of time. The model is used to build a more comprehensive process model (CHAPTER 5, page 89) and in the execution of experiments to investigate phenomena. Details of both these applications are contained in subsequent chapters.

4.1 IDENTIFICATION

The model being described in this chapter is identified as follows:

Name: Slag Bath Crust Conductor Model

Abbreviation: SBCC model

4.2 PROBLEM DEFINITION

The main objective of this study was to investigate the dynamic interaction between the freeze lining and slag bath in an ilmenite-smelting furnace. Part of this objective was to determine whether the eutectic groove present in the $FeO-TiO_2-Ti_2O_3$ ternary system is the reason for the compositional invariance observed in high-titania slag (Pistorius, 2002). This requires that slag solidification and melting in the furnace be modelled as completely as possible. The phase equilibria that are active during solidification and melting change the composition of the slag bath. These changes may be strong enough to cause the mentioned compositional invariance.

The magnitude of the influence of solidification and melting on slag bath composition could partially be determined by the surface area over which solidification and melting occur. The larger the area, the larger this influence could possibly be. Solidification and melting are known to occur in two zones in the furnace. Firstly the freeze lining zone that was described in the previous chapter. Secondly, a crust forms on the surface of the slag bath when the energy and material inputs to the furnace are switched off. This crust starts to melt away again when furnace operation resumes.

It was required to model the thickness, composition and temperature of the crust as functions of time, and, in the case of composition and temperature, as functions of position in the crust.

Because both slag bath temperature and composition are known to have an important influence on the solidification and melting of solid slag, the model had to be able to address both these aspects. The differences between heat transfer from the slag bath surface when the furnace is operational and when it is not, also had to be incorporated into the model.

4.3 SYSTEM DESCRIPTION

Figure 8 (page 13) can again be used as a view of the system currently being considered. In this case the surface of the slag bath is the area being focussed upon.

During normal operation, the slag bath surface is liquid and reductant particles are expected to float on the slag surface. The zone directly underneath the electrode is violently mixed by the momentum that is discharged from the arc and feed material.

Once the furnace is shut down, the thick cloud of dust that is present in the furnace freeboard during normal operation is sucked out by the off-gas system. This drastically increases the rate at which the slag bath can transfer heat to the furnace roof and walls by radiation (Reynolds, 2002). Heat therefore starts leaving the slag bath at a significant rate when the furnace is shut down. In addition to this, some slag reduction still takes place due to reaction between slag and reductant particles, and between slag and carbon dissolved in the metal bath. These endothermic reactions further lower the slag bath temperature. Once the furnace power has been turned off for some time, the slag bath surface starts to crust over.

When the furnace is switched on again, additional energy must be supplied to melt away the crust before normal operation can continue.

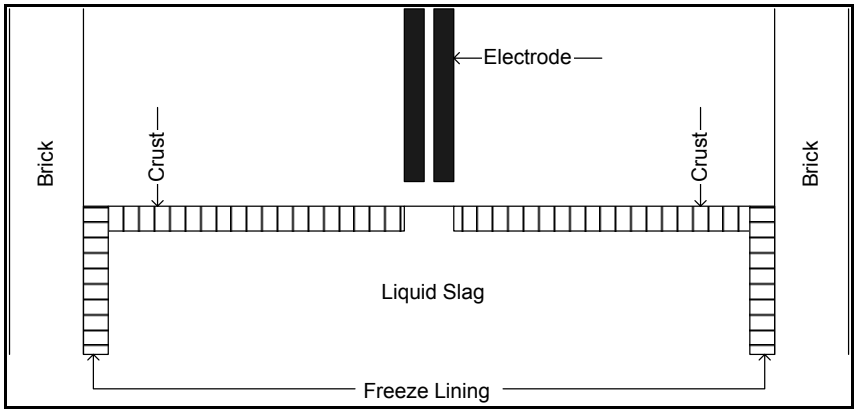

Figure 38 – Schematic representation of the slag bath and crust region of the furnace.

Figure 38 shows the region considered by the model in more detail. The region filled with vertical lines is the crust modelled with the SBCC model. The reason for the hole in the middle of the crust directly underneath the electrode is discussed in a subsequent paragraph.

4.3.1 System Geometry

If one only focuses on the crust shown in Figure 38, the system to be modelled is cylindrical. For this reason, phenomena occurring in the furnace will be identified and described based on the cylindrical coordinate system and therefore the following geometrical dimensions:

- Radial dimension
- Axial dimension
- Angular dimension

4.4 KEY PHENOMENA

To be able to model a process, one at least needs to be aware of all or most of the phenomena that are active in the process. For this reason, the next few paragraphs aim to identify most of the phenomena that are relevant to the system being considered in this chapter. It also aims to classify these phenomena in terms of their importance to the SBCC model.

4.4.1 Heat Transfer

a. Radial heat transfer

When a crust exists in the furnace it is likely that there will be a radial heat transfer component inside the crust. The reason for this is that the centre of the slag bath is generally hotter compared with regions closer to the walls. This generates a driving force for radial heat transfer. These heat transfer vectors are believed to be relatively small due to the low thermal conductivity of the material and the length of the conduction path from the radial centre to the outer radial limit at the wall.

Once the furnace power is switched back on after a crust had formed, the region under the electrode once again becomes the hottest region in the furnace. This will heat up the radial centre of the crust as well, inducing driving forces for radial heat transfer. In this situation it is again believed that the radial heat transfer components will be small compared with axial components due to the same reasons mentioned above.

It is believed that the magnitude of the radial components of heat transfer vectors within the crust is significantly smaller than that of the axial components discussed below. Due to this, radial heat transfer was seen as being less important than axial heat transfer (Assumption 4.1, page 70). It was not believed to be a key phenomenon within the context of the SBCC model.

b. Axial heat transfer

When the furnace is switched off and the freeboard emptied of the thick dust cloud that is present during normal operation, the rate at which heat is radiated to the furnace roof and walls increases dramatically (Reynolds, 2002). When considering the top 1 cm layer of the slag bath, the radiation and convection boundary conditions at the top of this layer will induce significant driving forces for axial heat transfer. This extraction of heat from the slag bath top surface does not cause formation of a crust immediately, but as time passes and the slag bath temperature drops, a crust eventually starts to form.

In this crust, axial heat transfer will remain dominant. The crust will initially be thin, with its lower surface in contact with hot liquid slag and its upper surface losing heat via radiation and convection to the furnace roof and walls. With such a temperature gradient across a fairly small axial distance, it is not difficult to envisage that axial heat transfer is of greatest importance. This dominance remains in place for the duration of most down time occurrences on the furnace. It is only when the axial dimension becomes comparable to the radial dimension that radial heat transfer would be of the same order of magnitude as axial heat transfer. This is however not likely to happen since the furnace should not be off for long enough periods of time to result in the formation of such a thick crust.

The important components of axial heat transfer when a crust is not yet present are as follows:

- Forced convection heat transfer in the slag bath transporting heat to and from the surface due to stirring in the bath.
- Radiation from the slag bath surface to the furnace roof and walls.
- Natural convection from the slag bath surface into the furnace atmosphere.

When a crust is present, the important components of axial heat transfer are:

- Forced/natural convection heat transfer transporting heat to and from the crust's lower surface due to stirring in the bath.
- Conduction through the crust.
- Radiation from the crust's upper surface to the sidewalls and roof.
- Forced/natural convection from the crust's upper surface to the furnace atmosphere.

Axial heat transfer, including all the components listed above, was seen as a key phenomenon since modelling of this phenomenon was crucial to the usefulness of the SBCC model. This is due to solidification and melting of the crust moving the interface between crust and slag bath primarily in the axial dimension.

c. Angular heat transfer

Because the slag bath surface is some distance above the level of the slag tap holes, it is likely that strong symmetry around the central vertical axis of the furnace exists. It is believed that the slag bath surface in the vicinity of the tap holes may be influenced by the tap holes, but also that this influence should be small. Such influences will result in angular temperature gradients that will induce angular heat transfer components. These components were believed to be insignificant within the context of the SBCC model (Assumption 4.1, page 70).

d. Heat sources

The following known heat sources are found in the system or influence the system as boundary conditions:

- Electric arc

  The electric arc heats the furnace atmosphere, slag bath and metal bath directly. This heat reaches the crust via convection and radiation.

  This heat source was seen as key to the SBCC model.

- Slag solidification

  When slag solidifies on the surface of the slag bath or the lower surface of an already existing crust, heat associated with the phase change is liberated.

  This heat source was seen as key to the SBCC model because the liberated heat must be accounted for in a heat transfer model of the crust. Ignoring it would have resulted in a serious weakness in the model.

- Chemical reaction

  Various chemical reactions (to be discussed in more detail below) can occur in the system. Some of these reactions are exothermic and therefore act as heat sources.

  This heat source was seen as key to the SBCC model for reasons similar to those quoted for the heat liberated during slag solidification.

e. Heat sinks

The following known heat sinks are found in the system or influence the system as boundary conditions:

- Slag melting

  When material melts away on the surface of the crust, heat associated with the phase change is absorbed.

  This heat sink was seen as key to the SBCC model for the same reasons as the slag solidification heat source.

- Chemical reaction

  Various chemical reactions (to be discussed in more detail below) can occur in the system. Some of these reactions are endothermic and therefore act as heat sinks.

  This heat sink was seen as key to the SBCC model for the same reasons as the slag solidification heat source.

4.4.2 Mass Transfer

a. Convective mass transfer

Due to movement in the slag and metal baths that is induced by the impinging arc, entering feed material, electromagnetic forces and buoyancy forces, slag is transported to and from the slag bath surface.

Convective mass transfer was not seen as a critical/key phenomenon to the SBCC model. The reason is that it is assumed that the slag bath is well mixed due to the momentum transferred to it by the above-mentioned forces (Assumption 4.2, page 70).

b. Diffusion

Due to compositional gradients inside the metal and slag baths it is expected that diffusion occurs in these zones.

Compositional gradients can also exist in the crust due to slag of different compositions having solidified at different axial positions. Such gradients also induce diffusion.

Diffusion was not seen as a critical/key phenomenon to the SBCC model. The reason for this is again the strong stirring effects that are present in the metal and slag baths. In the case of the crust it was simply assumed that mass transfer does not have a significant impact on the behaviour of the crust. Ideal mixing in the liquid, with no diffusion in the solid, corresponds to the assumptions of the Scheil model of solidification (Flemings, 1997).

4.4.3 Momentum Transfer

a. Slag and metal baths

Momentum is transferred to the slag bath by the impinging arc, material fed through the centre of the electrode, and by electromagnetic and buoyancy forces. This results in movement in the slag bath. This

movement can influence the rates at which heat and mass is transferred to and from the slag bath surface and the crust.

Momentum transfer in the slag bath was seen as important phenomena for the model under consideration since it can significantly influence heat transfer at the lower surface of the crust. This phenomenon therefore had to be addressed in the model. It was however believed that it would be adequate to incorporate this phenomenon as a simple boundary condition without modelling it in any great detail.

4.4.4 Chemical Reaction

This paragraph refers back to the description of chemical reactions provided for the FLC model. The major difference between the freeze lining and the crust is that the radial dimension is the focus in the case of the freeze lining, and the axial dimension in the case of the crust. Other than that the descriptions done for the FLC model are completely relevant here.

a. Reaction between liquid slag and liquid slag

Refer to paragraph 3.4.4a on page 32.

b. Reaction between liquid slag and solid slag

Refer to paragraph 3.4.4b on page 32.

c. Reaction between solid slag and solid slag

Refer to paragraph 3.4.4c on page 32.

4.4.5 Summary of Key Phenomena

			Level of importance to current modelling effort		
			1	2	3
Heat transfer	Radial	In slag bath	✔		
		Slag bath to freeze lining	✔		
		In freeze lining	✔		
		Freeze lining to refractory brick	✔		
		In refractory brick	✔		
		Refractory brick to ramming material	✔		
		In ramming material	✔		
		Ramming material to steel shell	✔		
		In steel shell	✔		
		Steel shell to water	✔		
	Axial	In slag bath		✔	
		Slag bath to crust			✔
		In crust			✔
		Out of crust top surface			✔
	Angular	In slag bath	✔		
		In crust	✔		
	Heat sources	Electric arc			✔
		Slag solidification			✔
		Chemical reaction			✔
	Heat sinks	Slag melting			✔
		Chemical reaction			✔
Mass transfer	Convection	In slag bath	✔		
	Diffusion	In slag bath	✔		
		In crust	✔		
Momentum	Slag bath			✔	

transfer	Metal bath		✔				
Chemical reaction	Liquid slag	With liquid slag	✔				
	Liquid slag	With solid slag					✔
	Solid slag	With solid slag	✔				

Table 4 – Summary of key phenomena for the SBCC model.

4.5 APPROACH AND MODEL COMPLEXITY

From the table summarising key phenomena it can be concluded that axial heat transfer, heat sources and sinks, and chemical reaction are of greatest importance to the SBCC model. Among these the heat-related phenomena are most basic to the problem being studied. The reason is that the thermal phenomena drive the chemical reactions that take place. Increase in temperature results in melting and decrease in temperature results in solidification. It must however also be stated that variations in slag bath composition without temperature variations could have the same influences.

Due to the general importance of heat-related phenomena in the system, heat transfer was used as the foundation of the model. The chemical reactions were modelled within the heat transfer framework where applicable.

4.5.1 Modelling of Heat Transfer

Because radial and angular heat transfer were identified to be of significantly less importance than axial heat transfer, and because this model was the first attempt at building a mathematical representation of the system, it was decided to model heat transfer in the axial dimension only. The model was therefore one-dimensional with the axial dimension being labelled the 'focus dimension'.

The range of radial positions in the furnace that were used, were chosen to start at a distance equal to the radius of the graphite electrode away from the radial centre furnace up to some short distance away from the inner surface of the furnace wall.

The reason for not starting at the centre of the furnace was to avoid having the arc influence the one-dimensional crust model when the furnace is started up. The arc can transfer heat directly to the liquid slag bath through the hole in the crust. This is a simplification that was used to avoid having to consider a second dimension (Simplification 4.1, page 71).

The reason for ending the radial dimension some distance from the wall was because the FLC model described in the previous chapter would typically be used together with the SBCC model in a complete process model of the furnace. Defining the radial range of the SBCC to stop some distance away from the wall prevented the two models from overlapping. This is also a simplification (Simplification 4.2, page 71).

The angular range used is the entire circumference of the furnace. The influence of tap holes was ignored in this model.

The range of the axial dimension that was used started at top of the slag bath and ended some distance below this surface. The distance that the model's axial dimension extends into the slag bath was chosen in such a way that there was room for the interface between the slag bath and crust to move sufficiently (by solidification and melting) to achieve the desired experimental results.

a. Solution method

A finite difference method was used to solve the heat transfer problem. An explicit formulation was used.

4.5.2 Modelling of Chemical Reaction

Modelling of chemical reactions relevant to the crust was done in the same way as it was done for the FLC model. Refer to paragraph 3.5.2 on page 35. The relevant assumption in the case of the SBCC model is Assumption 4.4 (page 70).

4.6 MODEL FORMULATION

4.6.1 Assumptions

The following paragraphs list assumptions made as part of the SBCC model formulation. The paragraphs clarify why the assumptions were made, their validity and the impact that the assumptions have on the model.

a. Assumption 4.1

Statement: Radial and angular heat transfer components are negligible and can be ignored.

Justification: This assumption is required to simplify the model. A one-dimensional model is significantly simpler and more manageable compared with two- and three-dimensional models.

Validity: The assumption is not completely true, since the existence of radial and angular heat transfer components can easily be proven. It is however true that the axial heat transfer components should be significantly larger than the radial and angular components. It was therefore acceptable given the objectives of the current work.

Impact: This assumption causes inaccuracies in the predictions of the model. These inaccuracies were viewed as being in balance with other uncertainties (measurement inaccuracies, uncertainty about dimensions, and uncertainty about material properties) in the process, and they were therefore viewed as not being significant within the context of the SBCC model and its current application.

b. Assumption 4.2

This assumption is the same as Assumption 3.2 of the FLC model. The reader is therefore referred to page 36 for detail.

c. Assumption 4.3

Assumption 3.3 of the FLC model applied to the crust layer is relevant here. Refer to page 36 for detail.

d. Assumption 4.4

Assumption 3.4 of the FLC model applied to the interface between slag bath and crust is relevant here. Refer to page 36 for detail.

e. Assumption 4.5

Assumption 3.5 of the FLC model applied only to liquid and solid slag is relevant here. Refer to page 37 for detail.

f. Assumption 4.6

Assumption 3.6 of the FLC model is relevant here. Refer to page 37 for detail.

g. Assumption 4.7

Assumption 3.7 of the FLC model applied to the crust layer is relevant here. Refer to page 37 for detail.

4.6.2 Simplifications

The following paragraphs list simplifications that were made in the model. The justification and impact of the simplifications are also presented.

a. Simplification 4.1

Description: The inner radial limit of the crust is defined to start a distance equal to the radius of the graphite electrode away from the radial centre.

Justification: This simplification was made to avoid having to consider a second dimension (the radial dimension) when the furnace starts up after a crust had formed. The arc can simply transfer its heat through the hole left in the crust directly below the electrode.

Impact: The simplification introduces inaccuracies into the model, but since the surface area of the region under the electrode that is effectively ignored by the crust model is small relative to the remaining bath surface area, the inaccuracies were acceptable.

b. Simplification 4.2

Description: The outer radial limit of the crust is defined to end some distance away from the inner surface of the furnace refractory wall.

Justification: This simplification was made to avoid overlap between the FLC model and the SBCC models when these models are used together in a larger process model.

Impact: The simplification introduces inaccuracies into the model, but since the surface area of the region next to the wall that is ignored by the crust model is small relative to the remaining bath surface area (between 4% and 13% of the total bath area for typical freeze lining thicknesses), the inaccuracies were tolerable.

4.6.3 Material Definitions

The definitions of the Liquid Slag and Solid Slag materials used in the SBCC model are identical to the definitions used for the FLC model. The reader is therefore referred back to the definitions made in the chapter on the FLC model.

a. Liquid Slag

Refer to paragraph 3.6.3a on page 39.

b. Liquid Metal

Refer to paragraph 3.6.3b on page 39.

c. Solid Slag

Refer to paragraph 3.6.3c on page 40.

4.6.4 Model Structure

The SBCC model is primarily a one-dimensional heat transfer model. The final structure of this model is now defined. Because of the confidentiality of actual furnace parameters, the author devised a set of furnace dimensions for use in the current work. It was attempted to choose the dimensions in such a way that the results of this work are relevant to industrial furnace operations.

Heat transfer was modelled by dividing the zone shown in Figure 39 into finite-difference nodes in the axial dimension. The boundaries between these nodes are indicated with horizontal dotted lines. A heat balance was then performed on each node during each time step. An explicit finite difference formulation was used.

In contrast with the FLC model, this model only had one layer making up the conductor. It was called the crust layer and abbreviated as CL.

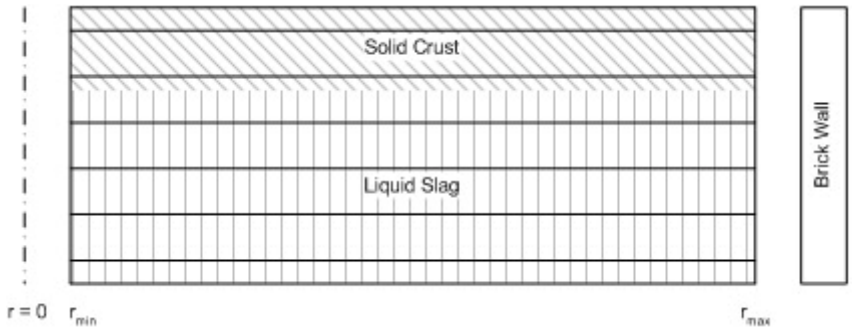

Figure 39 – Representation of the finite-difference model used to describe the crust.

a. Geometry and dimensions

Coordinate system: Cylindrical

Focus dimension: Axial

The axial dimension range and therefore the crust layer dimensions given below are typical values as these are adjusted to suit specific experimental objectives.

Dimension ranges:	Dimension	Min.	Max.	Units
	Radial:	0.030	4.425	m
	Axial:	0.000	1.000	m
	Angular:	0.0	2π	radians
Layer dimensions:	Layer	Min.	Max.	Units
	Crust layer:	0.000	1.000	m

Standard node size:	Layer	Size	Units
	Crust layer	0.010	m

The dimensions of the Crust Layer can be adjusted so that it includes the entire slag bath. If this is done, the entire volume of liquid slag will be able to participate in the calculation of solidification and melting equilibria. If some portion of the slag bath is excluded, that portion will not participate. By doing this, the model can be manipulated to be closer or further from complete (thermal) equilibrium in the slag bath. Excluding some portion of the slag bath becomes necessary when additional conductor modules are included in process model.

4.6.5 Heat Transfer

a. Boundary conditions

Because the conductor consists of only a single layer the number of boundary conditions is equal to two (the inner (lower) boundary in contact with liquid slag and the outer (upper) boundary representing the slag bath surface that is in contact with the furnace atmosphere).

- Crust layer outer surface boundary condition

  Type: Effective heat transfer coefficient

  Radiation and convection heat transfer are of importance at this boundary. Determining the magnitude of either of these components is difficult, especially for the conditions prevalent when the furnace is in operation. For this reason wall and roof heat losses on the furnace were used to determine an effective heat transfer coefficient.

  These boundary condition values were determined from a study on radiation heat transfer in the furnace freeboard (Reynolds, 2002). The results of that study were used to determine an estimate of the effective heat transfer coefficient. It was concluded from that work that the heat transfer coefficient could vary from 0.010 to 0.050 kW/(m^2.°C). The actual figures depend on numerous factors such as configuration of the sidewalls and roof, dust loading in the freeboard during operation, geometry of the roof, etc. A value of 0.019 kW/(m^2.°C) was decided upon for use while the furnace is operational, and 0.027 kW/(m^2.°C) when the furnace is off. In all cases 25 °C was used as the temperature towards which heat was transferred. This served as an estimate of the temperature of the cooling water on the outside of the sidewalls and roof. Because no actual plant data could be used for determination of the heat transfer coefficient, these rough estimates were used.

- Crust layer inner surface boundary condition

  Type: Ideal insulation

  No heat transfer was allowed over the inner surface of the crust layer. The reason is that heat is transferred into the crust layer by the bulk exchange of liquid slag with the slag bath. This is discussed in subsequent paragraphs.

b. List of symbols

SYMBOL	DESCRIPTION	UNITS OF MEASURE
$c_{p,material}(T)$	The heat capacity at constant pressure of the material identified by the subscript at temperature *T*.	kWh/(kg.°C)
ΔH_m^t	The increase (or decrease if negative) of the enthalpy of a finite-difference node identified by *m* from time step *t-1* to time step *t*.	kWh
ΔH_{FEM}^t	The enthalpy change associated with the equilibrium state calculated by the free energy minimiser.	kWh
ΔH_{ref}	The enthalpy of the material at the reference temperature of, in this case, 298.15 K.	kWh/kg
H_m^t	The enthalpy of finite-difference node *m* at time step *t*.	kWh
h_{eff}^t	Effective heat transfer coefficient at time step *t*.	kW/(m^2.°C)
$k_{material}(T)$	The thermal conductivity of the material identified by the subscript at temperature *T*.	kW/(m.°C)
M_{layer}	The number of finite-difference nodes in the layer identified by the subscript.	
m	An index identifying a finite-difference node. Nodes are indexed in ascending order as the position (radial, axial or angular) of the node increases.	
$R_{h_{eff}}^t$	The effective heat transfer coefficient resistance from the top of the slag bath surface of crust surface at time step *t*.	°C/kW
$R_{m,m'}^t$	The heat transfer resistance between finite-difference nodes *m* and *m'* at time step *t*.	°C/kW
$r_{\max,crust}$	The radial position of the outer radial surface of the crust layer.	m
$r_{\min,crust}$	The radial position of the inner radial surface of the crust layer.	m
T_∞^t	The temperature of the ambient environment at time step *t*.	°C
T_m^t	The temperature of finite-difference node *m* at time step *t*.	°C
t	Used as a superscript to indicate the current time step.	
V_m	The volume of finite-difference node *m*.	m^3
Δz_{layer}	The standard node size of the layer indicated by the subscript.	m
$\rho_{material}$	The density of the material identified by the subscript.	kg/m^3
$\Delta\tau$	The size of the integration time step of the model.	s

Table 5 – List of symbols used in CHAPTER 4 heat transfer formulation.

c. Crust layer outermost node heat balance

Change in enthalpy = Energy conducted into lower face
+ Heat generated within node
- Energy transferred via radiation and convection out of upper face

$$\Delta H_1^{t+1} = H_1^{t+1} - H_1^t = \frac{T_2^t - T_1^t}{R_{1,2}^t} \cdot \Delta\tau + \Delta H_{FEM}^t - \frac{T_1^t - T_\infty^t}{R_{h_{eff}}^t} \cdot \Delta\tau$$

$$H_1^t = \rho_{slag} \cdot V_1 \cdot \left[\int_{T_{ref}}^{T_1^t} c_{p,slag}(T)dT + H_{ref} \right]$$

$$V_1 = \pi \cdot \left(r_{\max,crust}^2 - r_{\min,crust}^2\right) \cdot \frac{\Delta z_{\mathrm{CL}}}{2}$$

$$R_{1,2}^t = \frac{\Delta z_{\mathrm{CL}}}{\pi \cdot \left(r_{\max,crust}^2 - r_{\min,crust}^2\right) \cdot k_{slag}\left(\frac{T_1^t + T_2^t}{2}\right)}$$

$$R_{h_{eff}}^t = \frac{1}{\pi \cdot \left(r_{\max,crust}^2 - r_{\min,crust}^2\right) \cdot h_{eff}^t}$$

ΔH_{FEM}^t represents heat associated with solidification and melting as calculated by Gibbs-free-energy minimisation.

d. Crust layer internal node heat balance

Change in enthalpy = Energy conducted into lower face
+ Heat generated within node
- Energy conducted out of upper face

$$\Delta H_m^{t+1} = H_m^{t+1} - H_m^t = \frac{T_{m+1}^t - T_m^t}{R_{m,m+1}^t} \cdot \Delta\tau + \Delta H_{FEM}^t - \frac{T_m^t - T_{m-1}^t}{R_{m,m-1}^t} \cdot \Delta\tau$$

$$H_m^t = \rho_{slag} \cdot V_m \cdot \left[\int_{T_{ref}}^{T_m^t} c_{p,slag}(T)dT + H_{ref}\right]$$

$$V_m = \pi \cdot \left(r_{\max,crust}^2 - r_{\min,crust}^2\right) \cdot \Delta z_{CL}$$

$$R_{m,m+1}^t = \frac{\Delta z_{CL}}{\pi \cdot \left(r_{\max,crust}^2 - r_{\min,crust}^2\right) \cdot k_{slag}\left(\frac{T_m^t + T_{m+1}^t}{2}\right)}$$

$$R_{m,m-1}^t = \frac{\Delta z_{CL}}{\pi \cdot \left(r_{\max,crust}^2 - r_{\min,crust}^2\right) \cdot k_{slag}\left(\frac{T_m^t + T_{m-1}^t}{2}\right)}$$

ΔH_{FEM}^t represents heat associated with solidification and melting as calculated by Gibbs-free-energy minimisation.

e. Crust layer innermost node heat balance

Change in enthalpy = Energy transferred into lower face
+ Heat generated within node
- Energy conducted out of upper face

$$\Delta H_{M_{CL}}^{t+1} = H_{M_{CL}}^{t+1} - H_{M_{CL}}^t = 0 + \Delta H_{FEM}^t - \frac{T_{M_{CL}}^t - T_{M_{CL}-1}^t}{R_{M_{CL},M_{CL}-1}^t} \cdot \Delta\tau$$

$$H_{M_{CL}}^t = \rho_{slag} \cdot V_{M_{CL}} \cdot \left[\int_{T_{ref}}^{T_{M_{CL}}^t} c_{p,slag}(T)dT + H_{ref}\right]$$

$$V_{M_{CL}} = \pi \cdot \left(r^2_{\max,crust} - r^2_{\min,crust} \right) \cdot \frac{\Delta z_{CL}}{2}$$

$$R^t_{M_{CL},M_{CL}-1} = \frac{\Delta z_{CL}}{\pi \cdot \left(r^2_{\max,crust} - r^2_{\min,crust} \right) \cdot k_{slag}\left(\frac{T^t_{M_{CL}} + T^t_{M_{CL}-1}}{2} \right)}$$

ΔH^t_{FEM} represents heat associated with solidification and melting as calculated by Gibbs-free-energy minimisation.

f. Liquid slag effective thermal conductivity

The liquid slag effective thermal conductivity was handled the same as in the FLC model. Refer to paragraph 3.6.5h on page 48.

4.6.6 Slag Solidification and Melting

Slag solidification and melting was handled the same as in the FLC model. Refer to paragraph 3.6.6 on page 48.

4.7 MODEL SOLUTION

4.7.1 Flow Sheet

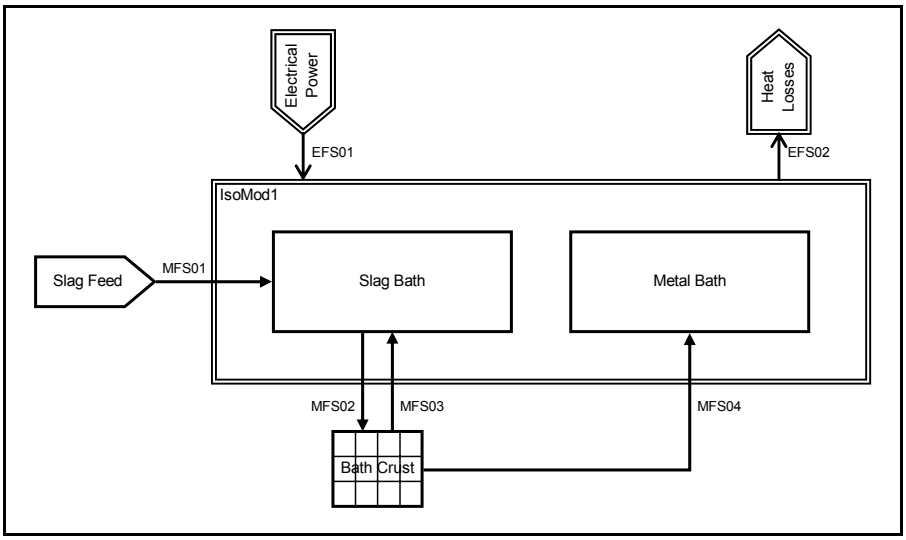

Figure 40 – Flow sheet of a simple process model incorporating the SBCC model.

Since the SBCC model used the slag bath only as a boundary condition, and the slag bath and its modelling were not included, the SBCC model could not be used on its own. It formed part of a larger modelling framework and always had to be incorporated into a larger model that was able to calculate the slag bath state. The modelling framework used for the construction of such models, is the one developed by Pauw (1989). A simple example is given in Figure 40. The remaining discussions about the SBCC model will be done within the context of the model presented in Figure 40.

See APPENDIX B for a description of the various model elements.

The elements of the flow sheet presented in Figure 40 are as follows:

- SlagFeed

  The SlagFeed material input module delivers liquid slag that is poured into the SlagBath mixer to establish an initial condition. The material produced by the SlagFeed material input module is discharged into the MFS01 material flow stream.

- MFS01

  The MFS01 material flow stream connects the SlagFeed material input module with the SlagBath mixer. It assists in establishing an initial condition.

- SlagBath

  The SlagBath mixer contains all liquid slag in the system.

- MFS02

  The MFS02 material flow stream connects the SlagBath mixer with the BathCrust conductor. It transports material that is about to participate in solidification and melting to the crust.

- BathCrust

  The BathCrust conductor is the single-layer SBCC model that is the main focus of this chapter.

- MFS03

  The MFS03 material flow stream connects the BathCrust conductor with the SlagBath mixer. It transports material that participated in solidification and melting from the crust.

- MFS04

  The MFS04 material flow stream connects the BathCrust conductor with the MetalBath mixer. It transports liquid metal that may form as a result of solidification and melting at the crust.

- MetalBath

  The MetalBath mixer contains all liquid metal in the system.

- ElectricalPower

  The ElectricalPower energy input module delivers electrical energy and represents a furnace electrical system.

- EFS01

  The EFS01 energy flow stream connects the ElectricalPower energy input module with the IsoMod1 isothermal module. In this simplified case, all energy from ElectricalPower reaches IsoMod1.

- IsoMod1

  The IsoMod1 isothermal module represents the slag and metal baths as an isothermal zone.

- EFS02

  The EFS02 energy flow stream connects the IsoMod1 isothermal module with the HeatLosses energy output module. All heat that is lost from the SlagBath and Metal Bath mixers by means other than conduction through the BathCrust conductor leaves IsoMod1 through EFS02.

- HeatLosses

  The HeatLosses energy output module represents all heat losses from the SlagBath and Metal Bath mixers other than the losses through the BathCrust conductor.

4.7.2 Initial Conditions

Before the step-by-step solution of the model was started, it was set up with the following initial conditions:

- The crust layer was set up with all nodes being empty and containing neither solid nor liquid slag.

4.7.3 Solution

The following procedure was used to solve the model during each time step:

- Fill the crust layer void with material from the SlagBath. The void refers to those nodes that do not contain any material. Upon start-up, this will include all Crust Layer nodes. Figure 41 shows the model solution procedure schematically for a time step where some solid slag is already present. Step (a) of Figure 41 shows the condition before filling the void, and step (b) the condition after filling the void.
- For the Crust Layer:
  - Calculate the enthalpy change for each node due to heat transfer and calculate the new temperature for each node. The result of this is indicated as step (c) of Figure 41. The temperature profile is now different.
  - Combine all liquid slag in the layer with a layer of solid slag. The result is shown in step (d) of Figure 41.
  - Calculate the equilibrium state of the combined material by Gibbs-free-energy minimisation. The result is shown in step (e) of Figure 41. More solid slag is now present and the combined material is isothermal.
  - Should any solid material result from the equilibrium calculation, this material is assigned to the outermost node m that is partially or completely void first, then to its inner neighbour $m+1$, then to $m+2$, etc. The result is shown in step (f) of Figure 41. A complete thermal profile has been applied to the Crust Layer.
  - Once the solid material has been distributed, the liquid resulting from the equilibrium calculation is used to fill the remaining empty or partially empty nodes. The result is shown in step (f) of Figure 41.
- Drain all liquid slag from the crust layer and add it back to the SlagBath. The result is shown in step (g) of Figure 41.
- Drain all liquid metal from the crust layer and add it to the Metal Bath mixer. For the sake of simplicity this is not indicated on Figure 19.
- Calculate new liquid slag composition and IsoMod1 temperature for the current time step (t).

This is not part of the SBCC model since the slag bath is simply assumed to be a boundary condition. It is done by other modules (SlagBath and IsoMod1) in the flow sheet.

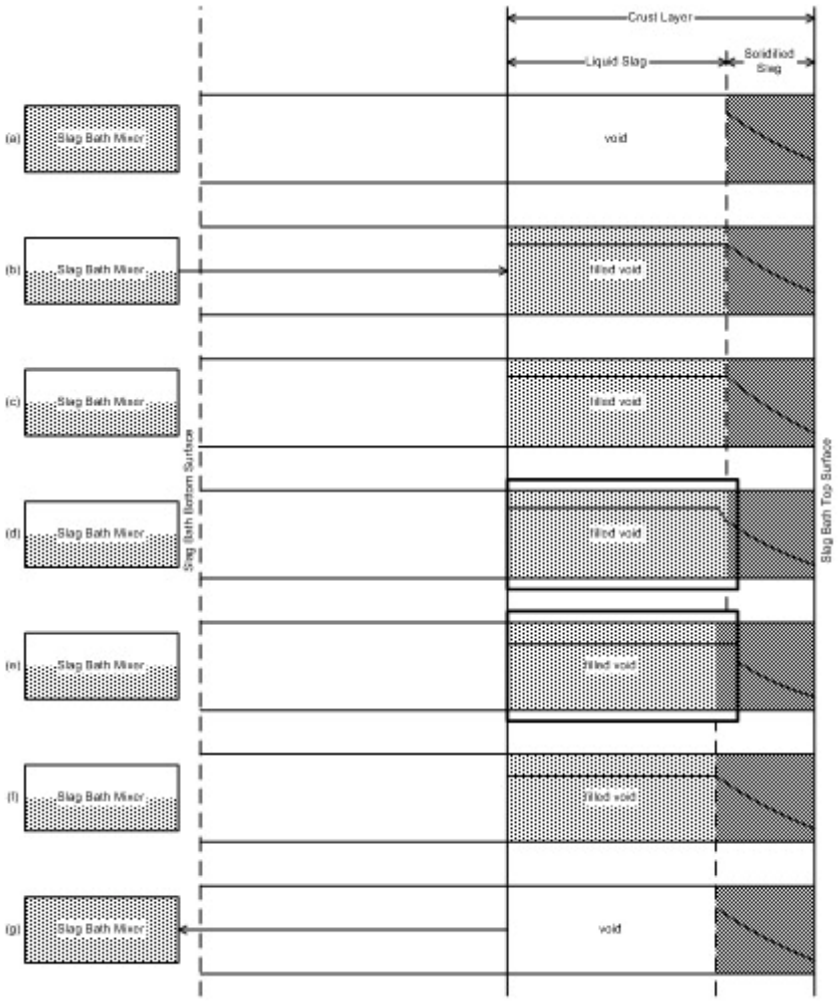

Figure 41 – Schematic representation of steps in the SBCC model solution procedure.

4.8 MODEL VALIDATION

4.8.1 Purpose

The purpose of validation is to verify the numerical integrity of the SBCC model (Thomas and Brimacombe, 1997).

4.8.2 Objectives

Model validation had to achieve the following objectives:

- Confirm the integrity of the basic heat transfer calculations.
- Confirm that the combination of the ChemApp Gibbs-free-energy-minimisation routine and the thermochemical data files used by the model calculate realistic equilibrium results.
- Confirm that the model is able to achieve solidification and melting of the freeze lining.

4.8.3 Methodology

The same ChemApp Gibbs-free-energy-minimisation routine and thermochemical data files used for the FLC model are used for the SBCC model. These were also assumed to be valid after the validation was performed for the FLC model.

Because there are differences (boundary conditions, number of layers) between the final FLC and SBCC models, the validation results of the FLC model could not be assumed to prove the validity of the SBCC. A number of experiments using the model shown in Figure 40 (page 76) therefore had to be done to inspect whether the results displayed the expected behaviour or not. If the slag bath is simply allowed to cool down, solidification is expected. If adequate amounts of energy are added to the slag bath, the crust is expected to melt away.

The heat transfer calculations included in the model were again validated by checking steady state results generated by the model against a set of analytically calculated steady state results. Example results of the analytical calculation are shown in Figure 42 and Figure 43.

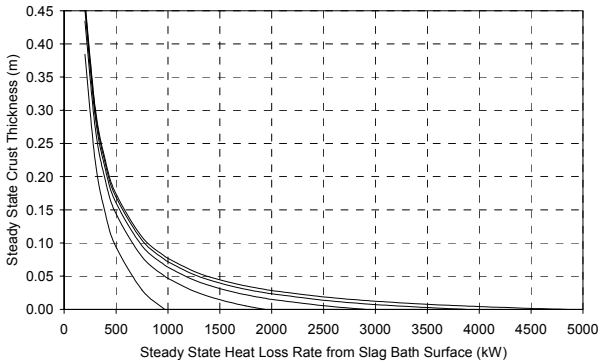

Figure 42 – Analytically calculated steady state crust thickness vs. heat loss rate from slag surface.

The left-most line represents an effective heat transfer coefficient of 0.010 kW/(m^2.°C). It is followed to the right by lines for 0.020, 0.030, 0.040 and 0.050 kW/(m^2.°C).

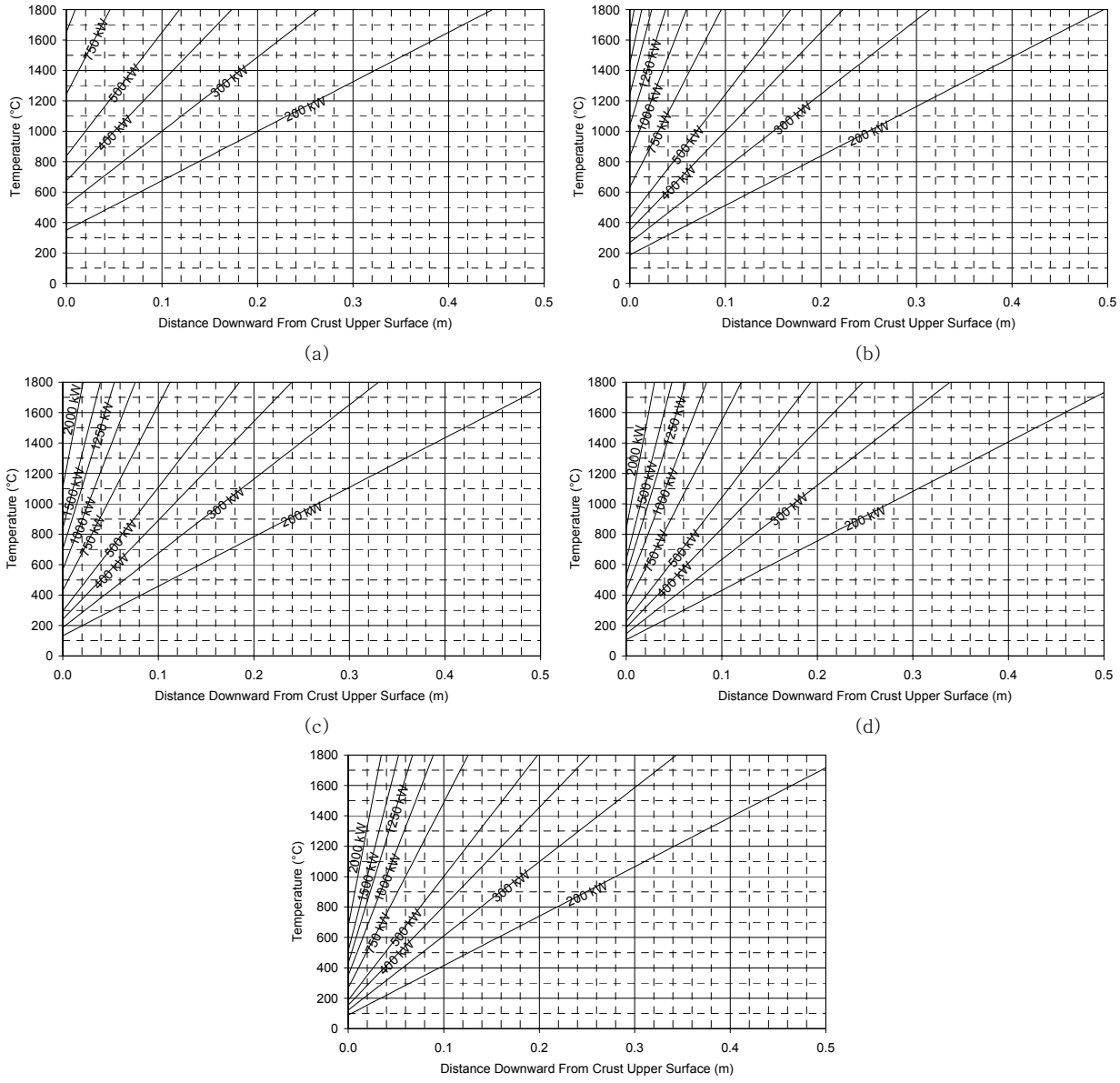

Figure 43 – Analytically calculated steady state temperature profiles in the crust layer.

Graph (a) was constructed with an effective heat transfer coefficient of 0.010 kW/(m^2.°C), (b) with 0.020 kW/(m^2.°C), (c) with 0.030 kW/(m^2.°C), (d) with 0.040 kW/(m^2.°C) and (e) with 0.050 kW/(m^2.°C).

The results generated by the comparison between model results and analytically calculated results were also used to achieve the last validation objective. Because a change in input heat flow rate caused the crust to either become thicker in the case of a reduced input heat flow rate or thinner in the case of an increased input heat flow rate, these experiments demonstrated whether the model was able to describe solidification and melting of the crust.

4.8.4 Validation Experiments

a. Experiment 4.1

Objective: Confirm the integrity of the model's heat transfer equations, and that the model is able to describe solidification and melting of the crust.

Initial condition: Fill up the SlagBath with a 10%-60%-30% (FeO-TiO_2-Ti_2O_3 mass percentages) slag at a temperature of 1635 °C. This temperature is just above the liquidus temperature of the slag. The slag composition is chosen to be on the rutile side of the eutectic groove. This means that rutile will be the primary phase that solidifies.

The effective heat transfer coefficient was set equal to 0.030 kW/(m^2.°C).

The model was started with no crust present.

Steps: Run the model with a heat flow rate of 3000 kW through the ElectricalPower energy input module until the model reaches a steady state. No crust was expected to form under these conditions.

Run the model with a heat flow rate of 1000 kW through the ElectricalPower energy input module until the model reaches a steady state. A crust was expected to form.

Run the model using the steady state results of the previous step as starting condition and apply a heat flow rate of 2000 kW through the ElectricalPower energy input module until the model reaches a steady state.

b. Experiment 4.2

Objective: Confirm the integrity of the model's heat transfer equations, and that the model is able to describe solidification and melting of the crust.

Initial condition: As for Experiment 4.1, but with a liquid slag composition of 10%-50%-40% (FeO-TiO_2-Ti_2O_3 mass percentages), and a liquid slag temperature of 1617 °C.

Steps: As for Experiment 4.1.

c. Experiment 4.3

Objective: Confirm the integrity of the model's heat transfer equations, and that the model is able to describe solidification and melting of the crust.

Determine the influence of a decrease in the effective heat transfer coefficient from the top of the slag bath or crust.

Initial condition: As for Experiment 4.1, but with an effective heat transfer coefficient of 0.020 kW/(m^2.°C).

Steps: Run the model with a heat flow rate of 2000 kW through the ElectricalPower energy input module until the model reaches a steady state. No crust was expected to form under these conditions.

Run the model with a heat flow rate of 500 kW through the ElectricalPower energy input module until the model reaches a steady state. A crust was expected to form.

Run the model using the steady state results of the previous step as starting condition and apply a heat flow rate of 1000 kW through the ElectricalPower energy input module until the model reaches a steady state.

d. Experiment 4.4

Objective: Confirm the integrity of the model's heat transfer equations, and that the model is able to describe solidification and melting of the crust.

Determine the influence of a decrease in the effective heat transfer coefficient from the top of the slag bath or crust.

Initial condition: As for Experiment 4.3, but with a liquid slag composition of 10%-50%-40% (FeO-TiO_2-Ti_2O_3 mass percentages), and a liquid slag temperature of 1617 °C.

Steps: As for Experiment 4.3.

4.8.5 Validation Results

Results of the validation experiments are presented below in the form of two graphs per experiment step. The graph on the left-hand side shows a comparison between an analytically calculated steady-state temperature profile of the furnace wall and freeze lining (solid line), and the same profile calculated by the SBCC model (crosses).

The second graph shows the difference between temperatures calculated by the SBCC model and analytically calculated temperature values. Positive values indicate overestimation by the SBCC model.

a. Experiment 4.1

%FeO	$\%TiO_2$	$\%Ti_2O_3$	$k_{liquid\ slag}$	$h_{effective}$
10	60	30	0.001 kW/(m.°C)	0.030 kW/(m^2.°C)

Step 1 of this experiment was executed with an ElectricalPower input of 3000 kW. The conditions modelled yielded no crust, as was expected. For this reason no graphs are shown for this step. The analytical calculation predicted a steady state slag bath temperature of 1650.6 °C. This was the temperature achieved by the model.

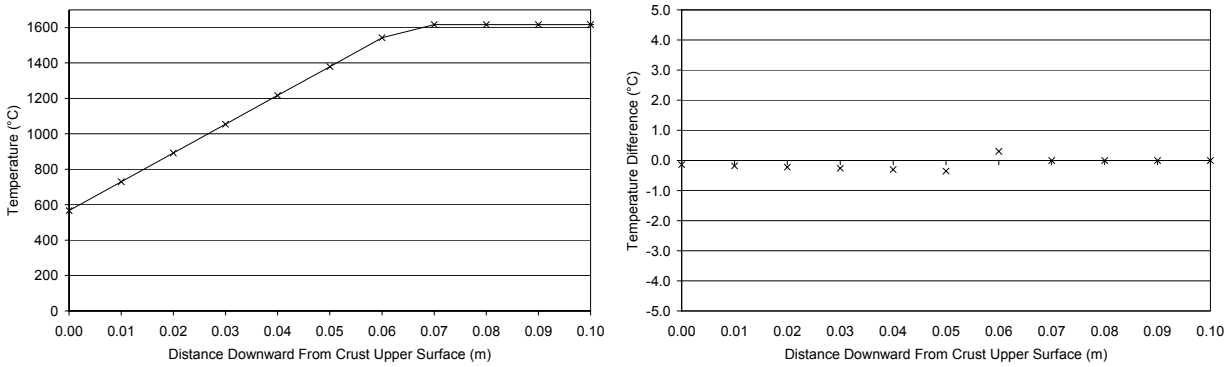

Figure 44 – Validation experiment 4.1 results for a heat input of 1000 kW.

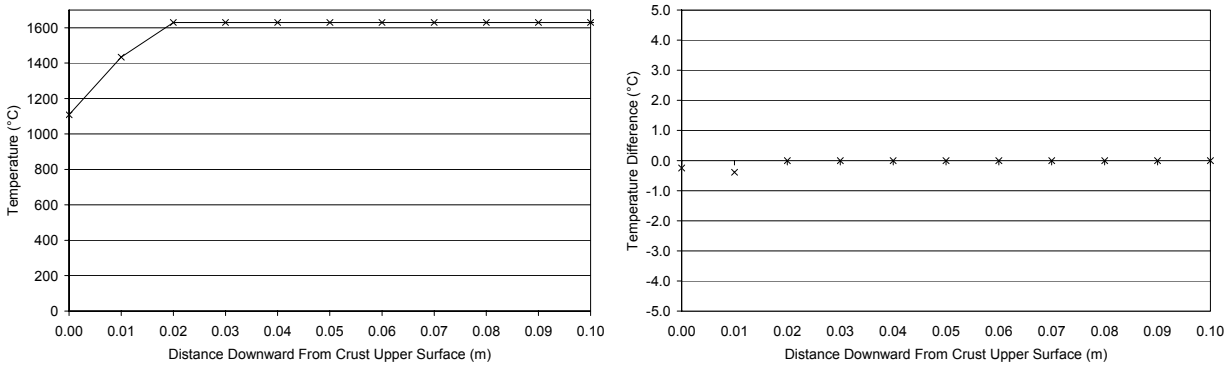

Figure 45 – Validation experiment 4.1 results for a heat input of 2000 kW.

b. Experiment 4.2

%FeO	%TiO_2	%Ti_2O_3	$k_{liquid\ slag}$	$h_{effective}$
10	50	40	0.001 kW/(m.°C)	0.030 kW/(m^2.°C)

Step 1 of this experiment was executed with an ElectricalPower input of 3000 kW. The conditions modelled yielded no crust, as was expected. For this reason no graphs are shown for this step. The analytical calculation predicted a steady state slag bath temperature of 1650.6 °C. This was the temperature achieved by the model.

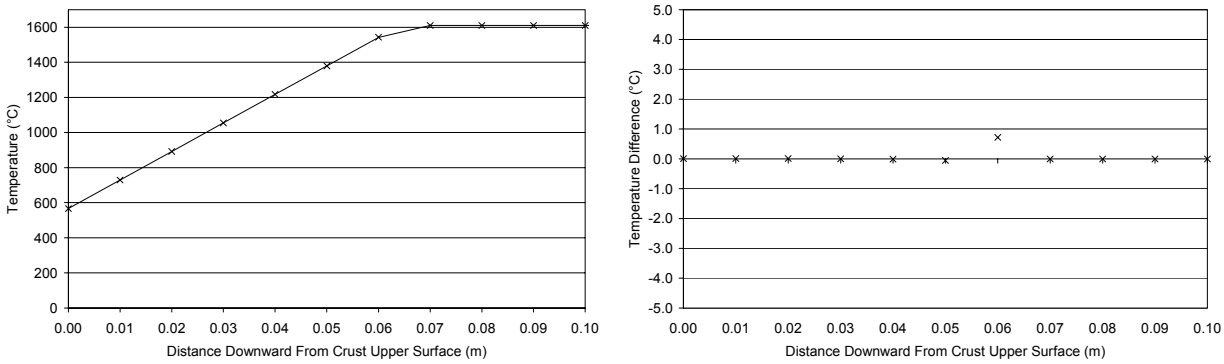

Figure 46 – Validation experiment 4.2 results for a heat input of 1000 kW.

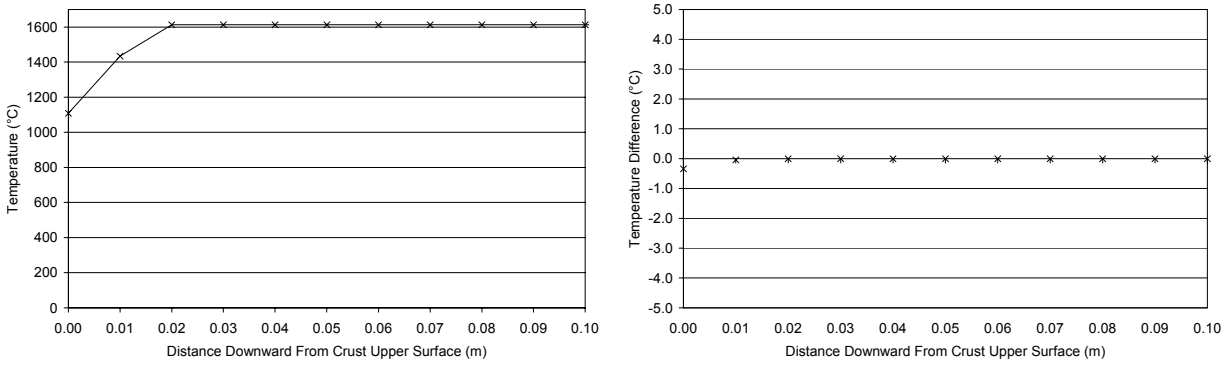

Figure 47 – Validation experiment 4.2 results for a heat input of 2000 kW.

c. Experiment 4.3

%FeO	%TiO_2	%Ti_2O_3	$k_{liquid\ slag}$	$h_{effective}$
10	60	30	0.001 kW/(m.°C)	0.020 kW/(m^2.°C)

Step 1 of this experiment was executed with an ElectricalPower input of 2000 kW. The conditions modelled yielded no crust, as was expected. For this reason no graphs are shown for this step. The analytical calculation predicted a steady state slag bath temperature of 1650.6 °C. This was the temperature achieved by the model.

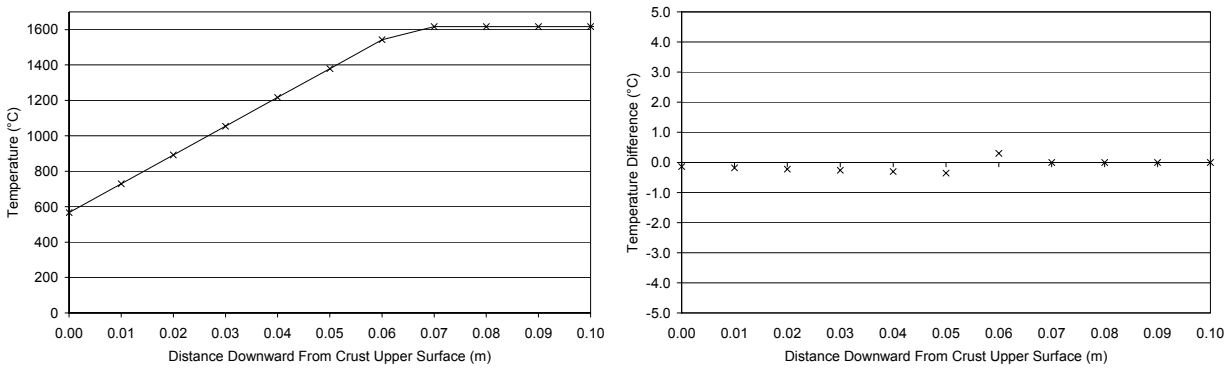

Figure 48 – Validation experiment 4.3 results for a heat input of 500 kW.

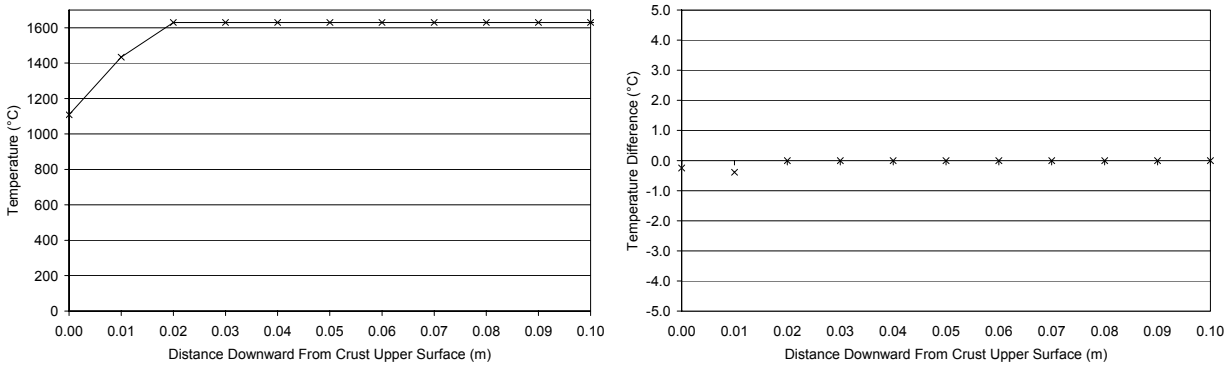

Figure 49 – Validation experiment 4.3 results for a heat input of 1000 kW.

d. Experiment 4.4

%FeO	%TiO_2	%Ti_2O_3	$k_{liquid\ slag}$	$h_{effective}$
10	50	40	0.001 kW/(m.°C)	0.020 kW/(m^2.°C)

Step 1 of this experiment was executed with an ElectricalPower input of 2000 kW. The conditions modelled yielded no crust, as was expected. For this reason no graphs are shown for this step. The analytical calculation predicted a steady state slag bath temperature of 1650.6 °C. This was the temperature achieved by the model.

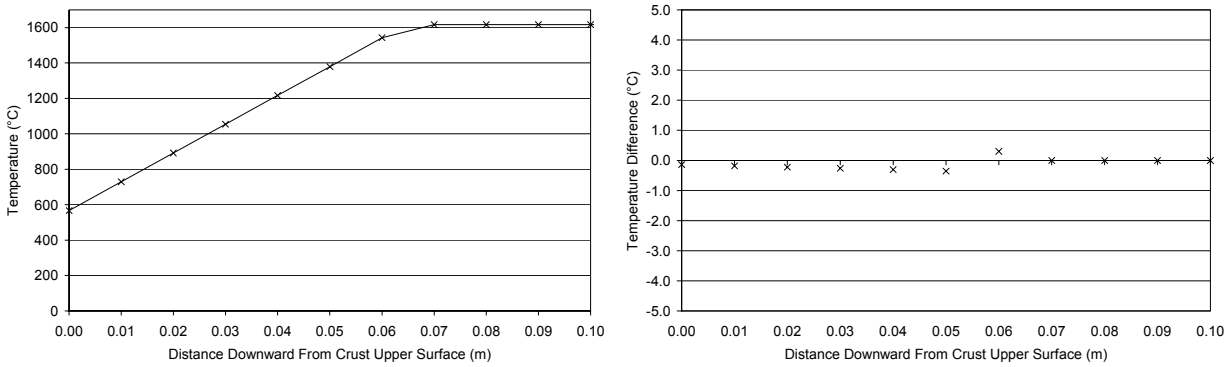

Figure 50 – Validation experiment 4.4 results for a heat input of 500 kW.

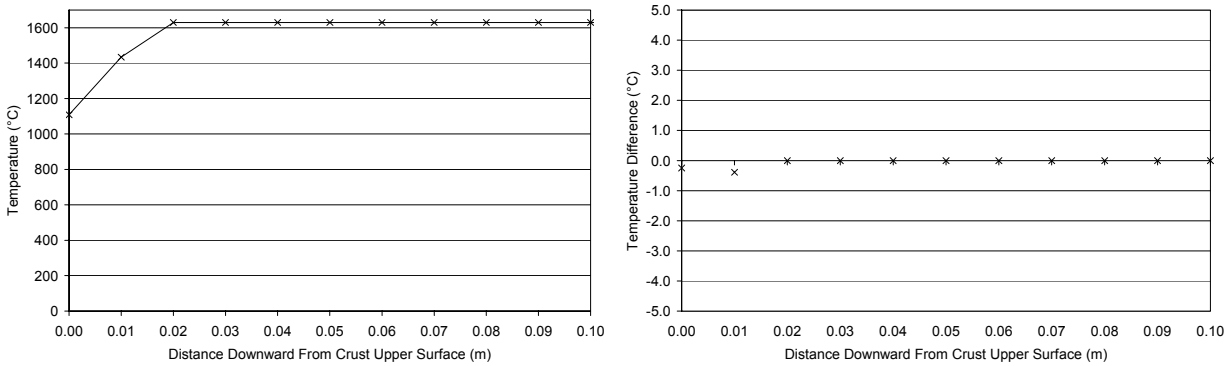

Figure 51 – Validation experiment 4.4 results for a heat input of 1000 kW.

e. Summary

Slag composition, steady state heat flow rate and effective heat transfer coefficient from the top of the slag bath or crust were the parameters covered by the validation experiments listed above. The model was able to reach steady state values that never deviated by more than 5 °C from the analytical solution. The deviations were believed to be due to round-off errors due to the ever-decreasing enthalpy change of the nodes as steady state is approached.

4.9 COMPARISON WITH ACTUAL DATA

Due to the confidentiality of most information pertaining to the industrial process, no comparison with actual data could be published here. The comparisons against analytically calculated values therefore serve as the only validation of the SBCC model.